Discontinuous Igneous Addition along the Eastern North American Margin beneath the East Coast Magnetic Anomaly

Collin C. Brandl[1], Lindsay Lowe Worthington[1], Maria Beatrice Magnani[2], Donna J. Shillington[3], Thomas W. Luckie[4]

[1] Department of Earth and Planetary Sciences, The University of New Mexico, Albuquerque, New Mexico 87131, USA

[2] Department of Earth Sciences, Southern Methodist University, Dallas, Texas 75275, USA

[3] School of Earth and Sustainability, Northern Arizona University, Flagstaff, Arizona 86011, USA

[4] Department of Earth Sciences, University of Southern California, Los Angeles, California 90089, USA

Corresponding author: Collin Brandl (cbrandl@unm.edu)

Key Points:

- High velocity lower crust beneath the East Coast Magnetic Anomaly is discontinuous and represents magmatic segmentation during rifting
- The extrusive:intrusive ratio at the ENAM is lower than the global average resulting in a significantly reduced total igneous volume
- The HVLC discontinuities are coincident to Mid-Atlantic Ridge fracture zones, potentially indicating a rift to ridge connection

Abstract

Detailed models of crustal structure at volcanic passive margins offer insight into the role of magmatism and distribution of igneous addition during continental rifting. The Eastern North American Margin (ENAM) is a volcanic passive margin that formed during the breakup of Pangea ~200 Myr ago. The offshore, margin-parallel East Coast Magnetic Anomaly (ECMA) is thought to mark the locus of synrift magmatism. Previous widely spaced margin-perpendicular studies seismically imaged igneous addition as seaward dipping reflectors (SDRs) and high velocity lower crust (HVLC; >7.2 km/s) beneath the ECMA. Along-strike imaging is necessary to more accurately determine the distribution and volume of igneous addition during continental breakup. We use wide-angle, marine active-source seismic data from the 2014-2015 ENAM Community Seismic Experiment to determine crustal structure beneath a ~370-km-long section of the ECMA. P-wave velocity models based on data from short-period ocean bottom seismometers reveal a ~21-km-thick crust with laterally variable lower crust velocities ranging from 6.9 to 7.5 km/s. Sections with HVLC alternate with two ~30-km-wide areas where the velocities do not exceed 7.0 km/s. This variable structure indicates that HVLC is discontinuous along the margin. Velocity-thickness analysis indicates that the HVLC discontinuity is the result of variable intrusion along-strike. Our results suggest that magmatism during early rifting was segmented and was lower in volume than previously thought. The HVLC discontinuities roughly align with locations of Mid-Atlantic Ridge fracture zones, which may indicate that early rift segmentation influenced later segmentation of the Mid-Atlantic Ridge.

Plain Language Summary

The East Coast of the United States is a passive margin that formed during continental breakup of Pangea, the most recent supercontinent. Although passive margins are generally not locales of active faulting and magmatism, by investigating their current structure, we gain insight into processes during past rifting. We know that extensive volcanism and magmatic addition to the Earth's crust occurred during the breakup of Pangea, but we do not fully understand how the distribution changes from north to south along the margin. To study these rocks, which are buried 10 – 20 km beneath the seafloor, we use ocean bottom seismometers that record human made sound waves to determine the sound speed of rocks beneath the surface, which depends on the specific type of rock. We found that the thickness and extent of magma-derived rocks are variable along the margin, with gaps up to 30 km wide. We think that the variability of these rocks is related to processes happening in the continental rift, and that it may have influenced the structure of the Mid-Atlantic Ridge that formed after rifting ended. We also estimate that the total volume of igneous rocks emplaced during breakup is significantly less than previously thought.

1. Introduction

Volcanic passive margins host significant volumes of igneous addition that are important not only for promoting continental rifting (Bialas et al., 2010; Geoffroy et al., 2015; Thybo & Nielsen, 2009), but also for global environment change and mass extinction events (Marzoli et al., 2018) and the understanding of mantle conditions and processes (e.g. Korenaga et al., 2002; Shuck et al., 2019). The volume and distribution of magmatism and its partitioning between the upper and lower crust during rifting is poorly known because there are limited datasets available to constrain 3D structure at

sites of breakup. Along-strike variability in margin structure can offer insight into syn-rift processes and potential connections between margin and mid-ocean ridge segmentation. Strike-perpendicular seismic imaging has constrained along-strike variability at passive margins on larger scales (e.g., Aslanian et al., 2021; Becker et al., 2014; Faleide et al., 2008; Holbrook & Kelemen, 1993; Klingelhoefer et al., 2009; Koopmann et al., 2014), but the paucity of along-strike imaging has prevented the necessary understanding of changes in crustal structure and magmatism along rifts.

The Eastern North American Margin (ENAM) is a volcanic passive margin that formed during the breakup of Pangea and opening of the Atlantic Ocean starting at ~200 Ma (Klitgord & Schouten, 1986) (Fig. 1). Crustal structure of the ENAM reflects the conditions of continental breakup, with records of extension and magmatism frozen into the current lithospheric structure. The ENAM has been considered an archetype for volcanic margins based on strike-perpendicular crustal structure containing seaward dipping reflectors (SDRs) and high velocity lower crust (HVLC; >7.2 km/s), which are both interpreted as igneous addition to the margin during rifting (e.g., Austin et al., 1990; Bécel et al., 2020; Holbrook & Kelemen, 1993; Shuck et al., 2019). The East Coast Magnetic Anomaly (ECMA), a large, positive amplitude anomaly that follows the ENAM from Florida to Nova Scotia, is sourced from the volcanic SDR package in the upper crust and has been interpreted as the rift-to-drift transition separating continental and oceanic crust (Alsop & Talwani, 1984; Behn & Lin, 2000; Davis et al., 2018; Greene et al., 2017) (Fig. 1). Along-strike variations in the width and amplitude of the ECMA suggest corresponding changes in rift structure and magmatism, potentially related to

segmentation of the Mid-Atlantic Ridge (Behn & Lin, 2000; Greene et al., 2017, 2020) (Fig. 1).

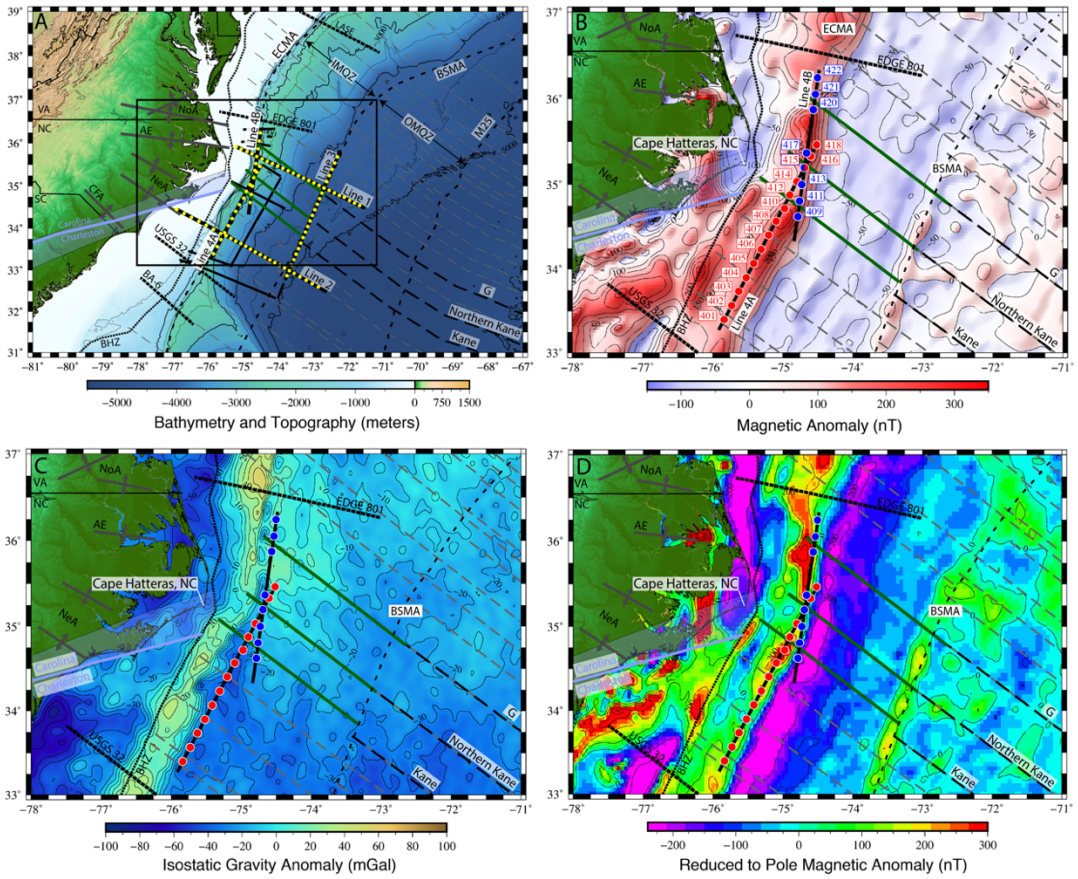

Figure 1) **Maps of the ENAM CSE study area with regional geologic and geophysical features.** *A)* Bathymetry and topography shown with the full ENAM CSE survey. Multichannel seismic reflection lines are shown by black solid lines, short period ocean bottom seismometer deployments are shown by yellow circles, and legacy seismic experiment lines EDGE-801, BA-6, USGS 32 and LASE are shown as black labeled lines. Fracture zone extrapolations of Klitgord and Schouten (1986) are shown as gray dashed lines and interpreted inner magnetic quiet zone offsets from Greene et al. (2017) are shown as green lines. Anomaly M25, the Blake Spur Magnetic Anomaly (BSMA), the Inner Magnetic Quiet Zone (IMQZ), and the Outer Magnetic Quiet Zone (OMQZ) are labeled. Onshore basement arches and the Carolina-Charleston terrane boundary are labeled. Black box represents the extent of the other maps. *B)* Zoom in on lines 4A and 4B of the survey with OBS instrument number labeled. Map shows EMAG2V3 (Meyer et al., 2017). *C)* Isostatic Gravity Anomaly (Behn and Lin, 2000). *D)* Reduced to Pole (RTP) magnetic anomaly (Behn and Lin, 2000).

In this study, we use traveltime tomography to model the P-wave velocity structure beneath the ECMA for a ~370-km-long along-strike section centered on Cape Hatteras, North Carolina. These models and subsequent analyses based on the velocity

103 structure offer insight into the crust beneath the ECMA and delineate along-strike
104 variability in crustal structure at scales of ~30 km which reflect early rifting structures.

105 ***1.1 Synrift Magmatism***

106 Igneous addition at continental rifts is often characterized by extensive surface
107 volcanism with localized intrusions into the crust or underplating at the base of the crust
108 (Bastow & Keir, 2011; Ebinger & Casey, 2001; Keranen et al., 2004; Thybo &
109 Artemieva, 2013). Synrift magmatism accommodates some extensional strain during
110 breakup and may be necessary for rifting, as modeling indicates that plate boundary
111 forces alone are too weak to break apart intact continental lithosphere (Bialas et al.,
112 2010; Buck, 2006). Igneous addition at volcanic margins, including the ENAM, the West
113 African Conjugate Margin, the southern West African Margin, and the South American
114 Margin, has been interpreted as a combination of volcanic flows (i.e., the SDRs) and
115 magmatic intrusions or underplating (i.e., the HVLC) (e.g., Aslanian et al., 2021; Becker
116 et al., 2014; Faleide et al., 2008; Holbrook & Kelemen, 1993; Klingelhoefer et al., 2009;
117 Koopmann et al., 2014).

118 Previous studies of the ENAM interpolated between widely spaced margin-
119 perpendicular profiles and assumed long wavelength (100 - >1000 km) along-strike
120 variability of crustal structure (Holbrook & Kelemen, 1993). However, smaller
121 wavelength (<100 km) variability in the magnitude and width of the ECMA implies that
122 there is significant variability in the thickness and extent of the anomaly's source body,
123 thought to be the SDR package, on smaller scales (Behn & Lin, 2000; Davis et al.,
124 2018; Greene et al., 2020). Recent magnetic modeling along the whole margin
125 interpreted multiple scales of magmatic segmentation along the margin based on

variability of the SDR package (Greene et al., 2020) (Fig. 1). In the vicinity of Cape Hatteras, NC, the magnetic source body changes broadly from thinner and wider in the south to thicker and narrower to the north, implying that Cape Hatteras is an important boundary along the margin (Greene et al., 2020). Constraining the full crustal structure beneath the ECMA has been difficult because there has been a lack of along-strike imaging at the ENAM and magnetic modeling does not offer insight into the lower crust. Along-strike imaging can illuminate variabilities in the lower crust at similar scales to those in the upper crust observed by whole margin modeling; if the SDRs and the HVLC were connected by the same magmatic plumbing system, we would expect significant variability in the thickness and extent of the HVLC correlated with SDR variability.

1.2 Segmentation of the ENAM

The relationship between segmentation of continental rifts and mature mid-ocean ridges remains unclear, but the crustal structure at rifted margins may hold crucial evidence that that connects them (Behn & Lin, 2000; Gerya, 2013; Greene et al., 2017; Illsley-Kemp et al., 2018; Taylor et al., 2009; Thomas, 2006). Continental rifts exhibit magmatic segmentation with sporadic intrusion and volcanism and/or structural segmentation with distinct fault systems (e.g., Ebinger & Casey, 2001; Hammond et al., 2011; Hayward & Ebinger, 1996). Mid-ocean ridge systems have characteristic segmentation with spreading segments bounded by oceanic transform faults that become fracture zones away from the ridge axis (Schouten et al., 1985). Rift segmentation may carry over to mature spreading centers based on the long wavelength variability of margin anomalies (Behn & Lin, 2000; Wyer & Watts, 2006), modeling of fracture zone formation (Gerya, 2013; Illsley-Kemp et al., 2018; Taylor et

al., 1995), structural correlation through multiple Wilson cycles (Thomas, 2006), or correlation between onshore and offshore structures (e.g., Franke et al., 2007; Koopmann et al., 2014).

The ECMA magnetic signature shows segmentation at multiple wavelengths (~600 – 1000 km and ~50 – 100 km) that may correlate with Mid-Atlantic Ridge segmentation (Greene et al., 2020). Along-strike segmentation of the SDR package interpreted in the south Atlantic margins and variability observed in the West African Coast Magnetic Anomaly also suggest a connection (Biari et al., 2017; Franke et al., 2007; Klingelhoefer et al., 2009; Koopmann et al., 2014). Relating structures along the ENAM to Mid-Atlantic Ridge segmentation is difficult because of the Atlantic Jurassic Quiet Zone, a region between M25 and the ECMA with no observable seafloor magnetic lineations (Behn & Lin, 2000; Greene et al., 2017) (Fig. 1). The combined lack of lineations and thicker abyssal sediments prevent tracing of Mid-Atlantic Ridge fracture zones in this region, so linear extrapolations based on plate motion have been used to approximate their locations at the ECMA (Behn & Lin, 2000). Recent analysis of the Inner Magnetic Quiet Zone (IMQZ) found faint lineations with offset that correspond to some extrapolated fracture zones, suggesting that there may be some segmentation structures at the ECMA that could be seismically imaged (Greene et al., 2017) (Fig. 1). Shuck et al. (2019) found no correlated structures along the Blake Spur Magnetic Anomaly, an indication that segmentation of the Mid-Atlantic Ridge may have developed after full lithospheric rupture. Previous to our study, magmatic segmentation at the ECMA was implied by Greene et al. (2020), but it remains unclear whether this early segmentation is recorded in the lower crustal structure.

2. Data and Methods

2.1 ENAM-CSE Line 4A and 4B

For this study we used ocean bottom seismometer (OBS) data from 23 stations acquired as part of the NSF-funded Eastern North American Margin Community Seismic Experiment (ENAM-CSE) in 2014 (Van Avendonk, 2015; Lynner et al., 2019). The OBSs recorded shots from the 36-element, 6600-in^3 array of the *R/V Marcus G. Langseth* along each profile (Fig. 1). We focus on Lines 4A and 4B located within the peak of the ECMA following the margin along-strike for ~370 km (Fig. 1). OBS gathers used for this study generally have a high signal to noise ratio with multiple arrivals evident and energy arriving from up to ~200 km offsets (Fig. 2). Stations A401-A406 have more complex arrivals within short offsets (< +-40 km) and have a near-offset first arrival with an apparent velocity of 6 km/s (much faster than typical sediment velocities) (Fig. 2). Picking arrivals between ~40 km and ~125 km source-receiver offset on stations A401-A406 was difficult due to low amplitudes and low coherency (Fig. 2). We attempted to include these arrivals in the inversions, but it was difficult to distinguish consistent phases and corresponding layer geometry, so only the first arriving, high energy phases were included in this area (Fig. 2). At offsets greater than ~125 km on these OBSs, amplitudes and coherency returned to normal levels and arrivals could be identified and picked (Fig. 2).

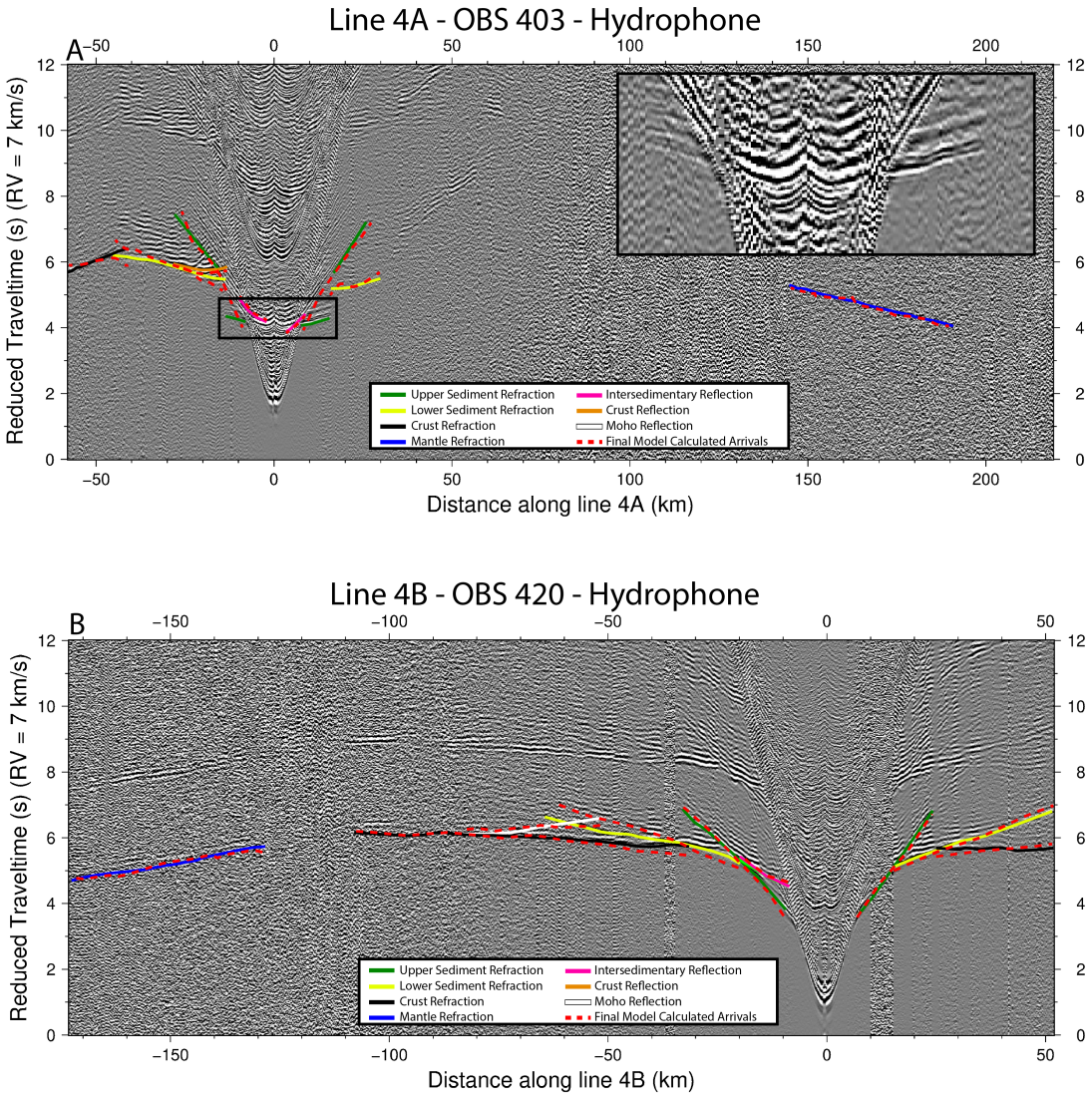

Figure 2) **Annotated ocean bottom seismometer data**. An OBS gather from Line 4A (station 403) (A) and Line 4B (station 420) (B) of the ENAM CSE plotted in distance along the line and reduced traveltime (with reduction velocity of 7 km/s). Traveltime picks (multicolor - see legend) and final calculated arrivals (red dashed) are plotted on top of data. Inset is an unpicked zoom onto the early, fast arrival caused by salt diapirism found on the southern end of line 4A.

We used a Butterworth bandpass filter on the OBS gathers to target frequencies between 4 and 15 Hz for general phase identification and interpretation, and between 10 and 25 Hz for near offset reflections. We identified seven phases for use in the velocity inversion that are similar to other recent refraction studies from the ENAM-CSE (i.e., Shuck et al., 2019), including an upper sedimentary refraction (Ps1), a lower

sedimentary refraction (Ps2), a crustal refraction (Pg), an upper mantle refraction (Pn), an inter-sedimentary reflection (PsP), a reflection from the top of the crust (PgP), and a Moho reflection (PmP). Uncertainties were assigned to all picked arrivals, ranging from 75 – 125 ms, based on source-receiver offset and visual inspection of signal-to-noise ratio. We used forward modeling of picks from each station and verified arrival reciprocity to quality control our traveltime picks before inversion.

2.2 Traveltime Tomography

We performed traveltime tomography with VMTomo following the methods of Van Avendonk et al. (2004) to iteratively invert our traveltime picks for subsurface P-wave velocities and boundary layer geometry. Our simple starting velocity models were based on results from crossing Lines 1 and 2 (Shuck et al., 2019) taken at the intersection points with Lines 4A and 4B and hung from the seafloor (Suppl. Fig. 1).

VMTomo first calculates raypaths and their respective traveltimes for each phase per shot point-OBS pair. The calculated travel times are compared to the corresponding picked traveltime, and the inversion then seeks to minimize the travel time residual by updating the velocity structure. The models were both constructed with 0.5 km by 0.2 km grid cells with no depth dependent changes in size. We chose a raytracing search radius of 0.2 km to match the vertical grid size and prescribed a regularization area of 20 km by 0.4 km with higher relative smoothing and a balanced regularization between boundary depths and velocities. In our analyses, the χ^2 error metric was decreased by ~50% with each iteration until a value of ~1 (indicating that the model misfit matches the prescribed uncertainty) was reached. We chose to apply a layer stripping approach, where we first inverted the shallowest layer to a χ^2 of 1 then moved to the next deepest

layer while holding everything above fixed. We verified the χ^2 of the entire model by running a final iteration with every phase at once.

We performed resolution tests and calculated derivative weight sum (DWS) on both velocity models to help guide our interpretations (Suppl. Figs. 2,4,5,6). Resolution results greater than ~50% for a given size test ellipse are considered acceptable for active source tomography of this kind (Van Avendonk et al., 2004). With the ray coverage for each line, the velocity models can reliably resolve large scale features (represented by an ellipse of 60 km by 8 km) on both lines within the sedimentary and crust layers except for the region between 0 and 100 km along Line 4A that has significantly low ray coverage (Suppl. Figs. 2,6). The velocity models can also reliably resolve small (10-km wide by 2-km tall) and medium scale features (30-km wide by 5-km tall) in the sedimentary layers and can resolve medium scale features in the crustal layer (Suppl. Figs. 4,5).

We estimated the uncertainty in our modeled crustal velocities and in the Moho velocity-depth tradeoff by perturbing our final model, raytracing the corresponding phases, and calculating a new χ^2. The crustal velocities have acceptable χ^2 values ($\leq$ 1.25) with perturbations from -0.05 – 0.07 km/s (Line 4A) and from -0.06 – 0.045 km/s (Line 4B) (Suppl. Figs. 7,8). For the velocity-depth tradeoff, the Moho reflection phase (PmP) has acceptable χ^2 values ($\leq$ 1.25) with depth perturbations from -0.28 – 0.85 km (Line 4A) and -1.5 – 0.78 km (Line 4B) and with velocity perturbations from -0.07 – 0.27 km/s (Line 4A) and from -0.2 – 0.29 km/s (Line 4B) (Suppl. Figs. 9,10).

3. Results

The final velocity models for Lines 4A and 4B have χ^2 values of 1.12 and 1.18, respectively, with RMS misfits of 101 and 108 ms (Fig. 3). The upper sedimentary layer on both lines has velocities ranging from 1.8 to 3.9 km/s and thicknesses ranging from ~2.0 to ~5.5 km. On Line 4A, between 0 km and 100 km along-strike, there are anomalously low velocities coincident to the OBS locations and a highly variable along-strike structure which we believe is due to previously identified salt diapirs that were observed on MCS reflection profiles (Dillon et al., 1982; Shillington et al., 2014; Tréhu et al., 1989) (Fig. 3). The low-quality data on OBS A401-A406 and the low ray coverage on the southern end of Line 4A are likely the result of these diapirs with very high seismic velocities relative to the surrounding sediment (Figs. 2,3 Suppl. Figs. 4,5,6). The lower sedimentary layers have velocities ranging from 2.9 to 5.9 km/s with thicknesses ranging from ~2.7 to ~5.0 km (Fig. 3). The crustal layers have velocities from 5.9 to 7.6 km/s with thicknesses from ~10.0 to ~13.0 km (Fig. 3). Velocities in the crustal layers have more along-strike variability than the other layers, including two anomalously low velocity regions between ~180 and ~210 km on Line 4A and between ~105 and ~130 km on Line 4B where velocities just above the Moho only reach 6.9 to 7.0 km/s (Fig. 3). Within the upper mantle, velocities range from 7.9 to 8.1 km/s with minimal along-strike variation. The layer boundary depths and seismic velocities generally agree with previous tomography results in other parts of the margin (e.g. Austin et al., 1990; Holbrook & Kelemen, 1993; LASE Study Group, 1986; Shuck et al., 2019). At the intersection point with Line 1 and Line 2 from the ENAM-CSE, the Moho on Lines 4A/4B is ~1-2 km deeper, which may represent slight differences in modeling

parameters (Shuck et al., 2019) or tradeoffs between lower crustal velocity and Moho depth (Suppl. Figs. 9,10).

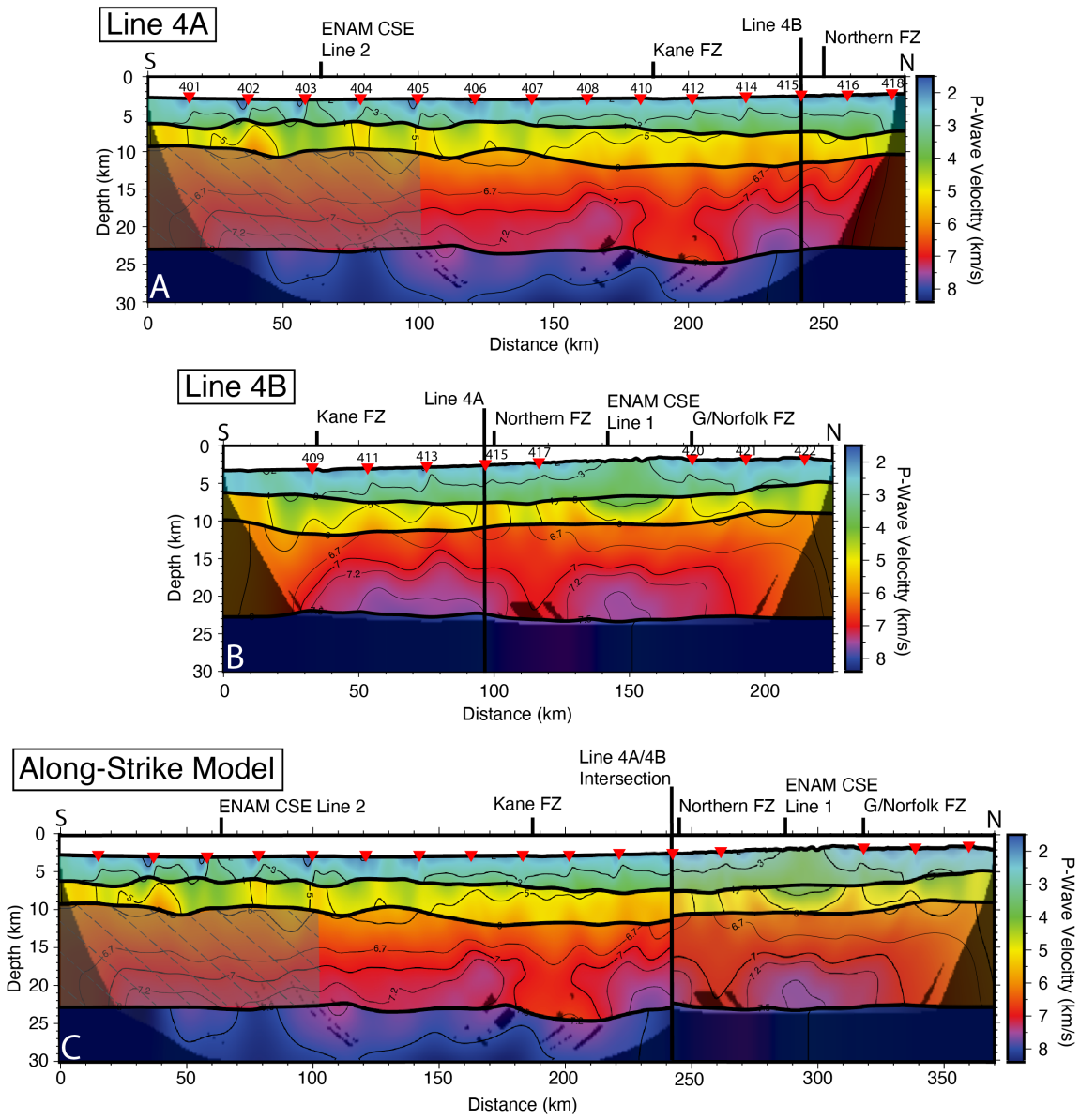

Figure 3) **Velocity modeling results**. Velocity models from Line 4A (A), Line 4B (B), and a combined along-strike model (C). P-wave velocities in each model are contoured and correspond to the color bar. Shaded and hatched region on Line 4A covers section of igneous crust with low ray coverage and resolution due to overhead salt diapirs. The combined along-strike velocity model was made with the portion of line 4A south of the intersection point and line 4B north of the intersection point.

To generate an along-strike view of the margin, we combined Lines 4A and 4B at their intersection point near Cape Hatteras, NC (Figs. 1,3). At the intersection point, velocities and boundary depths are in close agreement (Fig. 3). For this ~370-km-long section of the margin, the most along-strike variability is contained with the crustal layer. There is a slight thickening trends in the total crustal thickness and total sediment thickness from south to north, but this appears predominately related to shallowing bathymetry and the slight upslope orientation of Line 4B (Fig. 3, Suppl. Fig. 11). The lower velocity regions in the lower crust on Lines 4A and 4B at distances of ~180 km to ~210 km and ~245 km to ~285 km in the combined model are similar in size, but the area on Line 4B has a slightly higher velocity (6.9 km/s vs 7.1 km/s) (Fig. 3).

4. Discussion

4.1 Interpretation of the Velocity Model

The new P-wave velocity models along Lines 4A and 4B show detailed along-strike crustal structure beneath the ECMA for the first time, revealing significant variations in lower crustal velocity. The upper crustal velocity structure is also laterally heterogeneous, but changes in upper and lower crustal velocities are not tightly correlated. Our results fill in gaps between previous, sparse margin perpendicular observations and offer new insight into igneous addition during rifting and continental breakup.

To interpret igneous materials beneath the ECMA, we used isovelocity contours to approximate the areas of extrusive and intrusive addition. We use velocity contours as our best approximation for because there were no reflections observed in the OBS data that could delineate packages within the crust layer (Fig. 2) and initial processing

313 of coincident MCS reflection profiles from Lines 4A and 4B (Shillington et al., 2014)
314 showed little reflectivity within the basement that could be used to define boundaries. At
315 other volcanic margins, a lack of a mid-crustal reflection has been an indicator of
316 intrusion into the lower crust during rifting as opposed to underplating at the base of the
317 crust (Bécel et al., 2020; Eddy et al., 2014; Shuck et al., 2019; White et al., 2008).
318 Combined analysis of the wide-angle tomography results and MCS reflection profiles
319 from ENAM-CSE Lines 1 and 2 (Bécel et al., 2020; Shuck et al., 2019) show that the
320 upper portion of the SDR package in the MCS profile sits between the top of the crust
321 layer and the 6.5 km/s contour of the velocity model but these models did not image the
322 definitive base of the package. Along-strike variations in overburden can affect the
323 seismic velocities within the crust, we observe only small changes in sediment thickness
324 along-strike so this effect would be minimal (Fig. 3, Suppl. Fig. 11). Our uncertainty
325 analysis indicates that crustal velocities are well constrained with a depth uncertainty of
326 ~$\pm$0.5 km. Therefore, we use isovelocities to illuminate relative changes in both the
327 thickness of the volcanic layer and in the amount of synrift magmatic addition to the
328 lower crust in place of having a defined boundary.
329 Following previous investigators (e.g., Holbrook and Keleman, 1993; Shuck et
330 al., 2019), we used the 6.7 km/s contour to estimate the base of the extrusive (volcanic)
331 package and 7.2 km/s to estimate the top of the HVLC. With our isovelocity based
332 interpretation scheme, a volcanic package is present across both Lines 4A and 4B, with
333 a notable region between 210 km and 270 km along-strike where the 6.7 km/s contour
334 shallows to meet the top of the crust indicating significant thinning. HVLC is present on
335 both profiles except for two regions, from 170 – 220 km and 250 – 270 km in the along-

strike model, which have velocities less than ~7.2 km/s. We categorize these regions in the lower crust with reduced velocities as HVLC "gaps" because of the previously assumed prevalence of HVLC at the magma-rich ENAM (Fig. 3).

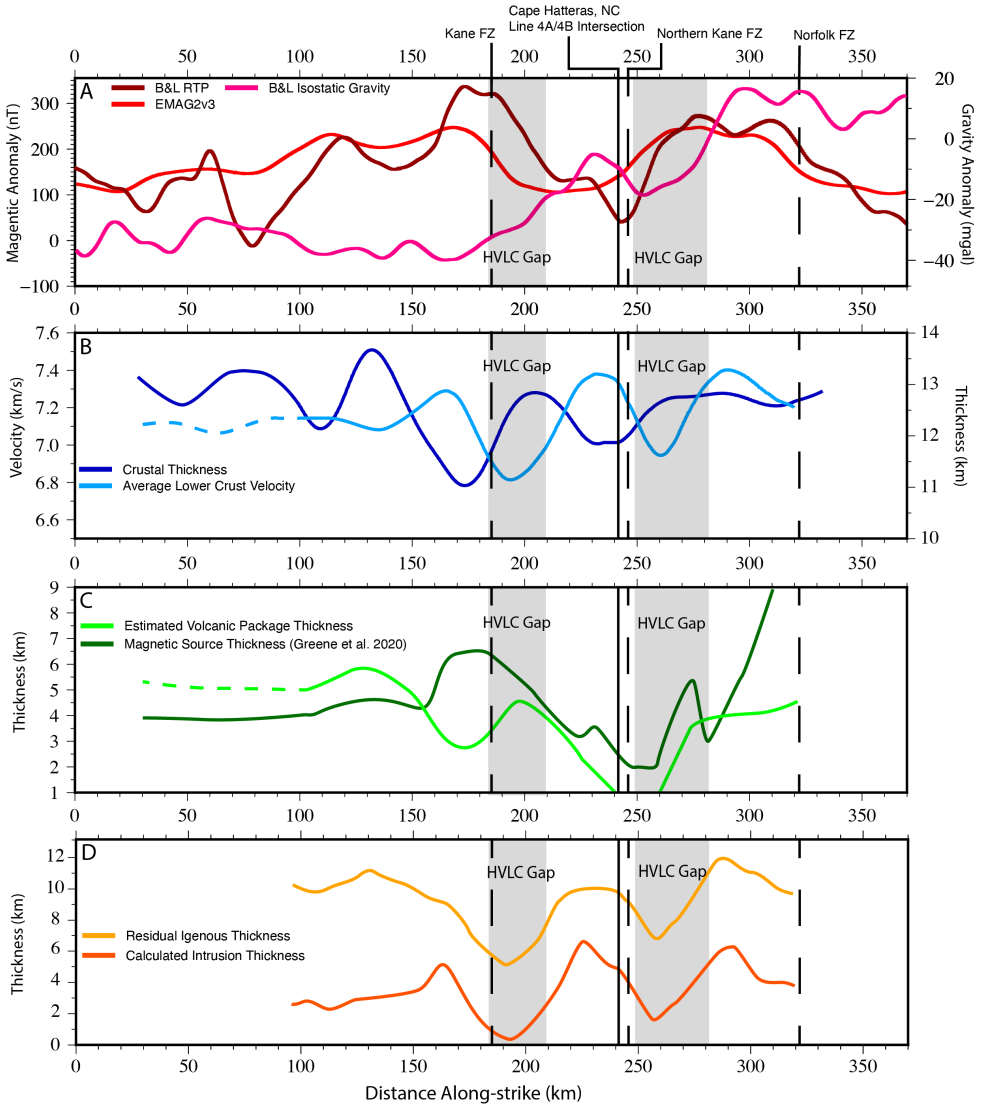

Figure 4) **Along-strike analysis**. Vertical lines show the location of the line 4A/4B intersection point, Cape Hatteras, NC, and the Kane, Northern Kane, and Norfolk fracture zones. Vertical gray boxes represent location of the HVLC gaps. *A)* Geophysical anomalies coincident to our along-strike model including EMAG2V3, the RTP magnetic anomaly from Behn and Lin (2000), and the isostatic gravity anomaly from Behn and Lin (2000). *B) Crustal* thickness along-strike, calculated from the top of the crust layer to the Moho and the average lower crustal velocity. *C)* Estimated volcanic package thickness, calculated from the top of the crust to the 6.7 km/s velocity contour and the modeled magnetic source thickness from Greene et al. (2020). *D) C*alculated intrusion thickness into the lower crust based on the linear mixing calculation of Marzen et al. (2020) and the residual igneous thickness determined by adding the intrusion thickness to the volcanic thickness (light green line in *C*).

To further contextualize our results, we compare with regional potential fields data (Fig. 4). The two-dimensional velocity models we present do not capture variable 3D structure that contributes to the potential fields, such that correlations between the two may be imperfect, but some general correlations may be expected. Magnetic and gravity anomalies along the ENAM show significant along-strike variation in amplitude (Figs. 1,4) that should reflect changes in the magnetic source body and density structure, respectively (e.g., Behn & Lin, 2000; Greene et al., 2020; Wyer & Watts, 2006). For the regions where we have reliable resolution, the reduced-to-pole (RTP) magnetic anomaly appears to broadly be positively correlated with the estimated volcanic thickness calculated from the top of the crustal layer to the 6.7 km/s contour (Behn & Lin, 2000) (Fig. 4). The general correlation is consistent with the volcanic package constituting the primary magnetic source (Austin et al., 1990; Davis et al., 2018; Greene et al., 2017, 2020). In terms of gravity, the northern HVLC gap correlates with a local minimum in the isostatic gravity anomaly but the southern HVLC gap does not (Behn & Lin, 2000) (Fig. 4). The isostatic anomaly should be sensitive to variations in density structure throughout the sediments, crust, and upper mantle, so the lack of correlation with the southern HVLC gap could be due to its location within a larger trend of decreasing gravity anomaly or 3D structures influencing the anomaly that that our 2D lines cannot capture (Fig. 4).

We also note that the estimated volcanic and HVLC thicknesses are not correlated along-strike (Figs. 3,4). For example, south of the 4A/4B intersection a thick section of volcanics overlies a section of crust without HVLC (Fig. 4). This observation is surprising because both surface volcanics and the HVLC represent igneous addition to

the margin derived from the same mantle melt, so we might expect to find the thickest volcanic sections above the thickest HVLC. Cape Hatteras, NC (coincident to the intersection point) represents a change in margin orientation (Fig. 1), early seafloor spreading regimes (Greene et al., 2017), and early rifting processes (Greene et al., 2020), but it is difficult to know if those long wavelength variations would affect the small-scale structure. While the upper and lower crust are both sourced from the same mantle melt, and they are correlated on larger scales (>500 km), our results suggest that the magmatic system is more complex at smaller scales.

4.2 Origin of the Lower Crust Beneath the ECMA

Previous studies that detected HVLC beneath the ECMA had considered it a continuous, tabular shaped feature for the length of ENAM (e.g., Holbrook & Kelemen, 1993). Considering the distribution of HVLC in our along-strike view and in the models from ENAM-CSE Lines 1 and 2 (Shuck et al., 2019), we suggest instead that the HVLC may be more sporadically distributed along the margin. However, the origin of this along-strike variability remains unclear. The crust beneath the ECMA is sandwiched between the extended continental crust of the Atlantic coast plain (Luckie, 2017; Guo et al., 2019) and continental shelf (Shuck et al., 2019) and anomalously thin, faulted, and seismically fast proto-oceanic crust (Bécel et al., 2020; Shuck et al., 2019). Bécel et al., (2020) interpreted the crust beneath the ECMA as extrusive upper crust with intermediate diking and lower crustal intrusion based on ENAM-CSE MCS profiles Lines 1 and 2 (Fig. 1), combined with collocated the wide-angle tomography (Shuck et al., 2019). Many other passive margins show similar structure based on strike-perpendicular seismic profiling (e.g Aslanian et al., 2021; Biari et al., 2017; Klingelhoefer

et al., 2009; Museur et al., 2021; White et al., 2008). Our observation that HVLC beneath the ENAM is discontinuous on ~30-km length scales, however, has not been observed at other margins with along-strike profiles (e.g., Aslanian et al., 2021; Contrucci et al., 2004; Klingelhoefer et al., 2009; Reuber et al., 2016).

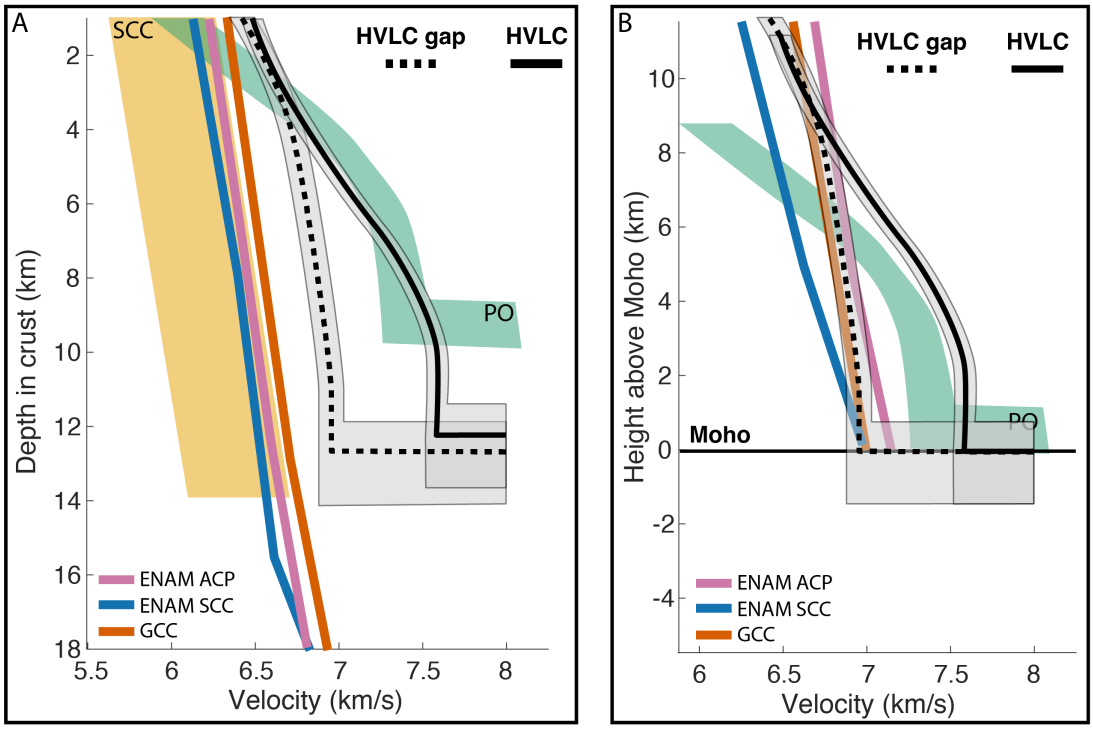

Figure 5) **One Dimensional Analysis**. Plots of the average 1D velocity profiles comparing the crust with HVLC and the crust with HVLC gaps to stretched continental crust (SCC) (Christensen and Mooney, 1995), proto-oceanic crust (PO) (Shuck et al., 2019), continental crust from the Atlantic Coastal Plain (ENAM ACP) (Luckie 2017), continental crust from southern Georgia (GCC) (Marzen at al., 2020), and stretched continental crust from Line 1 and Line 2 landward of the ECMA (ENAM SCC) (Shuck et al., 2019). 1D velocity profiles are hung from their respective top of the crust (*A*) and are aligned at their respective Moho as determined by the authors (*B*). Gray boxes around the HVLC and HVLC gap profiles reflect estimated uncertainties in the model's crustal velocities and Moho depth.

To further investigate the nature of the heterogeneous lower crust beneath the ENAM, we calculated the average velocity-depth profile for crust with and without HVLC on Lines 4A and 4B. We compared the 1D profiles with the proto-oceanic crust from Lines 1 and 2 of the ENAM CSE and with a range of continental crust profiles from the Atlantic Coastal Plain, the ENAM continental shelf, the south Georgia Basin, and a

404 global baseline (Christensen & Mooney, 1995; Luckie, 2017; Marzen et al., 2020; Shuck
405 et al., 2019) (Fig. 5).

406 When hung from the top of the crust, the average one-dimensional velocity-depth
407 profile for sections with and without HVLC have nearly identical upper crustal velocities
408 that are close to the upper proto-oceanic crust, which would also have a volcanic origin
409 (Fig. 5A). Velocities near the top of the crust are slightly higher than the equivalent
410 proto-oceanic crust, but this difference could be due to the thicker sediment load
411 beneath the ECMA closing fractures and raising the velocity (Fig. 5A). At ~4 – 5 km
412 depth, the HVLC profile diverges, reaching ~7.5 km/s at the Moho as opposed to ~6.9
413 km/s for crust without HVLC (Fig. 5A). The velocity profile for the HVLC gaps is located
414 in between the proto-oceanic crust and the continental crustal profiles providing an
415 unclear origin (Fig. 5A).

416 To compare lower crustal structure more directly, we align the one-dimensional
417 velocity profiles at the Moho, as interpreted by the authors of each respective study
418 (Fig. 5B). In this view, the HVLC gap profile falls within the range of lower continental
419 crust from eastern North America (Luckie, 2017; Marzen et al., 2020; Shuck et al.,
420 2019), suggesting that these sections represent lower continental crust that was not
421 intruded during rifting (Fig. 5B). Studies at other Atlantic passive margins have found
422 that the middle to lower continental crust may persist through extension becoming the
423 base of transitional margin crust (e.g. Aslanian et al., 2021; Biari et al., 2017; Contrucci
424 et al., 2004; Klingelhoefer et al., 2009). Based on this analysis, we suggest that the
425 along-strike variation in the lower crust velocity structure beneath the ECMA reflects

alternating sections of extensive and limited intrusion into lower continental crust (Fig. 6).

4.3 Igneous Addition During Continental Breakup

Volcanic margins are defined by a significant volume of igneous addition, and several previous studies have attempted to calculate the ENAM's total igneous volume. We first use our interpreted velocity models to approximate the proportion of extrusive and intrusive magmatism at the ENAM as this ratio is frequently used to estimate the total volume for the margin. A recent global analysis of volcanic rifted margins found an average thickness ratio of 1:3 between SDRs and HVLC, providing a baseline value for the ratio of extrusive to intrusive rocks (Gallahue et al., 2020). Observations in both active and failed rifts (e.g., the Midcontinent Rift (Elling et al., 2020), the Afar Rift (Bastow & Keir, 2011), and the Main Ethiopian Rift (Keranen et al., 2004)) and at volcanic passive margins (e.g., offshore Norway (Faleide et al., 2008), South America (Becker et al., 2014), and southwest Africa (Koopmann et al., 2014)) indicate that SDR:HVLC thickness ratios may vary along-strike, but there has not been a detailed along-strike analysis of the ratio at the ENAM.

By comparing our isovelocity derived thicknesses (e.g., Fig. 4), we find that the ratio between the volcanics and the HVLC in this part of the ENAM is 1:2$\pm$0.25 on average. However, this estimate assumes that the entire lower crust is fully formed from igneous addition, not heavily intruded continental crust. To refine our estimate, we calculated the along-strike igneous intrusion thickness into the crust using a linear mixing equation following the methods of White et al. (2008) and Marzen et al. (2020) (Fig. 4). Assuming a background lower crustal velocity of 6.8 km/s and a mafic intrusion

velocity of 7.5 km/s, the intrusion thickness ranges from ~0.5 km to ~6.5 km with local minimums coincident to the HVLC gaps (Fig. 4). Adding the estimated volcanic package thickness to the calculated intrusion thickness represents the total igneous thickness along-strike, which varies more significantly than the overall crustal thickness (Fig. 4).

The updated intrusion thickness reduces the extrusive:intrusive ratio to 1:1.25±.25 which is similar to the ratio determined by White et al. (2008) in the North Atlantic. Without a modeled reflector separating the volcanics and HVLC, our ratio is dependent on the specific isovelocity chosen as the proxy boundary. A different chosen velocity would result in a slightly different ratio, but our results indicate that the ratio is generally lower than previous estimates from ENAM and the recent global compilation from Gallahue et al. (2020).

Holbrook & Kelemen (1993) calculated a maximum igneous volume of ~3.2 x 10^6 km^3 using the cross-sectional area of imaged SDRs and HVLC on transects BA-6 and EDGE 801 multiplied by the margin length (Fig. 1). Greene et al. (2020) modeled the margin-wide ECMA magnetic source and used the SDR:HVLC relation of Gallahue et al. (2020) (SDR:HVLC = 1:3) to estimate a total volume of ~1.6 x 10^6 km^3, a 50% reduction. While the Greene et al. (2020) estimate accounts for variability along the margin, it relies on a global relationship that may not apply to the ENAM. Using our new calculated ratio along the entire margin, the Greene et al. (2020) estimate would reduce by ~48% to 8.39±0.93 x 10^5 km^3. In addition to the updated ratio, the observed discontinuities in HVLC along the rest of the margin would further reduce the volume by a potentially significant amount. However, it remains unclear how prevalent the HVLC discontinuities are along the ENAM. These volume estimates are not definitive, but add

to a growing body of evidence that magmatism during the formation of the ENAM was less voluminous and more irregularly distributed than previously thought (e.g., Bécel et al., 2020; Greene et al., 2020; Marzen et al., 2020; Shuck et al., 2019)

4.4 Magmatic Segmentation During Early Rifting

Our interpretation that there are variable degrees of intrusion beneath the ECMA provides evidence for along-strike magmatic segmentation during the rifting process (Figs. 6,7). We suggest that there were discrete sites of magmatic intrusion in the continental rift that correlate to the areas with HVLC while gaps between the magmatic centers remained unintruded (Fig. 7). Extensive volcanism covered the rift surface, sometimes flowing away from the magmatic centers to cover the unintruded crust, which is imaged now as the volcanic upper crust (Figs. 3,6,7).

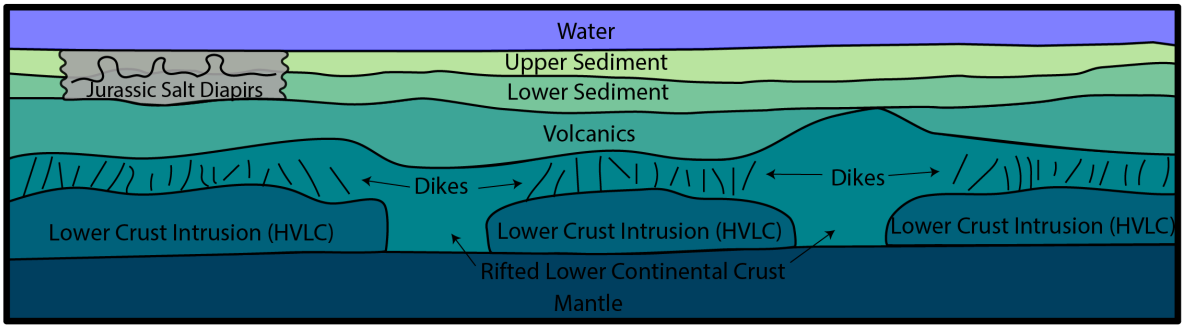

Figure 6) **Interpretation of the Crust.** Conceptual model of the along-strike geology beneath the ECMA with interpreted velocity models structures. The along-strike velocity model's crust layer is comprised of a volcanic package and intrusions into the lower crust (HVLC) with diking in between following interpretation by Becel et al., (2020). HVLC gaps in the velocity model are interpreted as rifted lower continental crust with no intrusion.

Magmatic segmentation has been observed in the active Main Ethiopian Rift and in the Afar Rift where significant volcanism and crustal intrusion occur in ~30 km to ~100 km long and ~20 km wide segments near the rift axis (Ebinger & Casey, 2001; Hammond et al., 2011; Hayward & Ebinger, 1996; Keranen et al., 2004). Velocities at

491 the ENAM are faster than in the East African Rift, perhaps reflective of more mature
492 crust with more significant magmatism at the ENAM (Hammond et al., 2011; Keranen et
493 al., 2004). Segmentation during early-stage rifting may also manifest by border faults,
494 some of which alternate in polarity, such as at the Midcontinent Rift or in the Malawi Rift
495 (Dickas et al., 1997; Scholz et al., 2020). Border-fault-defined segmentation may be
496 abandoned when magmatism and magmatic volatiles become involved and/or
497 extension migrates to other fault systems (e.g. Ebinger & Casey, 2001; Muirhead et al.,
498 2016).

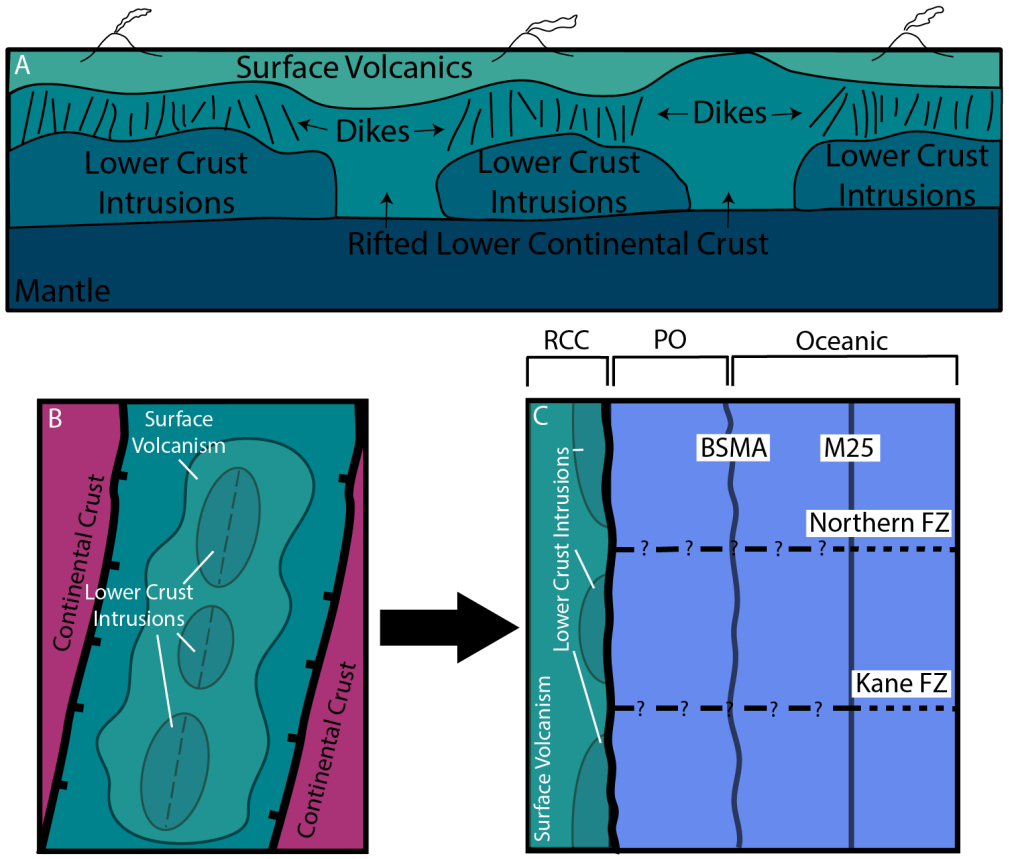

499

500 Figure 7) **Conceptual segmentation model.** A) A hypothetical cross section beneath the active
501 continental rift with developed magmatic segmentation (discontinuous lower crust intrusions) and
surface volcanics. B) Map view of the magmatic segmentation in the continental rift. C) The continental
502 rift evolved into the Mid-Atlantic Ridge with successful breakup, and the correlation of fracture zones
to the discontinuous HVLC gaps suggest a rift to ridge connection, but the fracture zones cannot be
traced directly to the ECMA. BSMA is Blake Spur Magnetic Anomaly. RCC is rifted continental crust. PO
is proto-oceanic crust defined by Shuck et al., (2019).

The cause of magmatic segmentation at the ENAM is unclear. In some locations segmentation may be driven by pre-existing structures that serve as zones of weakness, facilitating extension and magmatism (Frizon de Lamotte et al., 2015). The ENAM has experienced multiple Wilson cycles and exhibits evidence pointing to structural controls on segmentation (Thomas, 2006). However, in our study area, the segmentation we observe does not appear to correlate with pre-existing structures, including a suture zone and onshore basement arches (Figs. 1,3). Magmatic segmentation may also be driven by small scale convection in the upper mantle, providing a source of heat to weaken the lithosphere and a source of melt for magmatism (Gac & Geoffroy, 2009; Geoffroy et al., 2001). It is unclear if this would allow for the small-scale gaps we observe in the lower crust, or if it is more related to longer wavelength segmentation.

Notably, the observed along-strike variations in lower crustal structure are coincident with the westward extent of extrapolated fracture zones from the Mid-Atlantic Ridge, which indicates a possible connection between rift and ridge segmentation (Behn and Lin, 2000; Greene et al., 2017) (Figs. 3,4,7). Petrological-thermomechanical modeling from some passive margins and active rifts suggests that magmatism drives segmentation and that the rift segments can evolve directly into spreading segment, but it is unclear if this process occurred at the ENAM or the spatial correlation is a coincidence (Gerya, 2013; Illsley-Kemp et al., 2018; Taylor et al., 2009). The lack of fracture zone identification between M25 and the ECMA, excluding the faint lineation offsets observed by Greene et al. (2017), and the lack of correlated structures at the

BSMA (Shuck et al., 2019), make it difficult to draw a definitive conclusion (Figs. 1,7). Further imaging of the ENAM, or other passive margins, may illuminate additional along-strike variability in crustal structure and could provide stronger evidence of the rift to ridge connection which is crucial for our continued understanding of continental breakup and mid-ocean ridge formation.

5. Conclusions

1) New tomographically-derived seismic velocity models along the ECMA show that crustal structure is significantly more variable along-strike than previously thought, with most variability located in the lower crust. Two large “gaps” in HVLC are present in the lower crust where velocities reach ~6.9 - 7.0 km/s above the Moho compared to ~7.3 - 7.5 km/s within the HVLC.

2) The average one dimensional velocity structure of the HVLC “gaps” match rifted lower continental crust in velocity-depth space, indicating that these areas were not intruded or were minimally intruded during breakup. Therefore, the along-strike crustal structure beneath the ECMA consists of discrete regions of intrusion (the HVLC) and regions with very limited intrusion (the HVLC gaps) covered by a volcanic layer.

3) The average lower crustal velocity and the estimated extrusive igneous thickness are not correlated, indicating extensive surface volcanism regardless of lower crustal intrusions. We estimate that the igneous thickness along-strike, calculated with linear mixing, is ~2.5 km to ~6.0 km less than the than total crustal thickness.

4) The ratio of extrusive to intrusive thicknesses in the igneous crust beneath the ECMA is less than previously defined by global studies and strike perpendicular profiles. Our estimated ratio of 1 to 1.25±.25 lowers recent estimates of the ENAM's total volume by ~48%.

5) The along-strike crustal variability is on similar scales to observations made at active and failed continental rifts, implying that our observations reflect magmatic segmentation during early rifting. The magmatic segmentation approximately aligns with Mid-Atlantic Ridge fracture zones suggesting that segmentation of the rift could be related to segmentation of the ridge, but further along-strike imaging of the ENAM is needed to establish a definitive relationship.

DATA and ACKNOWLEDGEMENTS

The ENAM-CSE study area includes traditional lands and waters of many Indigenous peoples, including the Lumbee, Skaruhreh/Tuscarora, Hatteras, Roanoke and Chesapeake territories. The data used in this analysis is freely available at the Marine Geoscience Data System Portal under expedition code EN546: https://www.marine-geo.org/tools/search/Files.php?data_set_uid=27784 (doi: 10.1594/IEDA/500017). We thank the principal investigators of the ENAM-CSE, the captains and crews of the R/V *Langseth* and R/V *Endeavor*, and the many technicians, students and scientists that contributed to the community dataset acquisition. Masako Tominaga, John Greene, and Brandon Shuck provided constructive comments and discussion during preparation of

this manuscript. This work was supported by NSF awards OCE-1654804 to Worthington, OCE-1654781 to Magnani and OCE-1654629 to Shillington.

References

Alsop, L. E., & Talwani, M. (1984). The east coast magnetic anomaly. *Science*, *226*(4679), 1189–1191.

Aslanian, D., Gallais, F., Afilhado, A., Schnurle, P., Moulin, M., Evain, M., et al. (2021). Deep structure of the Pará-Maranhão/Barreirinhas passive margin in the equatorial Atlantic (NE Brazil). *Journal of South American Earth Sciences*, *110*(December 2020), 103322. https://doi.org/10.1016/j.jsames.2021.103322

Austin, J. A., Stoffa, P. L., Phillips, J. D., Oh, J., Sawyer, D. S., Purdy, G. M., et al. (1990). Crustal structure of the Southeast Georgia embayment-Carolina trough: Preliminary results of a composite seismic image of a continental suture (?) and a volcanic passive margin. *Geology*, *18*(10), 1023–1027.

Bastow, I. D., & Keir, D. (2011). The protracted development of the continent–ocean transition in Afar. *Nature Geoscience*, *4*(4), 248–250.

Bécel, A., Davis, J. K., Gibson, J. C., Shuck, B. D., Van Avendonk, H. J. A., & Gibson, J. C. (2020). Evidence for a Prolonged Continental Breakup resulting from Slow Extension Rates at the Eastern North American Volcanic Rifted Margin. *Journal of Geophysical Research: Solid Earth*, e2020JB020093. https://doi.org/10.1029/2020JB020093

Becker, K., Franke, D., Trumbull, R., Schnabel, M., Heyde, I., Schreckenberger, B., et al. (2014). Asymmetry of high-velocity lower crust on the South Atlantic rifted margins and implications for the interplay of magmatism and tectonics in continental breakup. *Solid Earth*, *5*(2), 1011–1026.

Behn, M. D., & Lin, J. (2000). Segmentation in gravity and magnetic anomalies along the US East Coast passive margin: Implications for incipient structure of the oceanic lithosphere. *Journal of Geophysical Research: Solid Earth*, *105*(B11), 25769–25790.

Bialas, R. W., Buck, W. R., & Qin, R. (2010). How much magma is required to rift a continent? *Earth and Planetary Science Letters*, *292*(1–2), 68–78.

Biari, Y., Klingelhoefer, F., Sahabi, M., Funck, T., Benabdellouahed, M., Schnabel, M., et al. (2017). Opening of the central Atlantic Ocean: implications for geometric rifting and asymmetric initial seafloor spreading after continental breakup. *Tectonics*, *36*(6), 1129–1150.

Buck, R. (2006). The role of magma in the development of the Afro-Arabian Rift System. *Geological Society, London, Special Publications*, 43–54. https://doi.org/10.1144/GSL.SP.2006.259.01.05

Christensen, N. I., & Mooney, W. D. (1995). Seismic velocity structure and composition of the continental crust: A global view. *Journal of Geophysical Research: Solid Earth*, *100*(B6), 9761–9788.

Contrucci, I., Matias, L., Moulin, M., Géli, L., Klingelhofer, F., Nouzé, H., et al. (2004).

Deep structure of the West African continental margin (Congo, Zaïre, Angola), between 5 S and 8 S, from reflection/refraction seismics and gravity data. *Geophysical Journal International*, *158*(2), 529–553.

Davis, J. K., Bécel, A., & Buck, W. R. (2018). Estimating emplacement rates for seaward-dipping reflectors associated with the US East Coast Magnetic Anomaly. *Geophysical Journal International*, *215*(3), 1594–1603.

Dickas, A. B., Mudrey, M. G., Ojakangas, R. W., & Green, J. C. (1997). Segmented structure of the middle Proterozoic Midcontinent rift system, North America. *SPECIAL PAPERS-GEOLOGICAL SOCIETY OF AMERICA*, 37–46.

Dillon, W. P., Popenoe, P., Grow, J. A., Klitgord, K. D., Swift, B. A., Paull, C. K., & Cashman, K. V. (1982). Growth Faulting and Salt Diapirism: Their Relationship and Control in the Carolina Trough, Eastern North America: Rifted Margins: Field Investigations of Margin Structure and Stratigraphy.

Ebinger, C., & Casey, M. (2001). Continental breakup in magmatic provinces: An Ethiopian example. *Geology*, *29*(6), 527–530.

Eddy, D. R., Van Avendonk, H. J. A., Christeson, G. L., Norton, I. O., Karner, G. D., Johnson, C. A., & Snedden, J. W. (2014). Deep crustal structure of the northeastern Gulf of Mexico: Implications for rift evolution and seafloor spreading. *Journal of Geophysical Research: Solid Earth*, *119*(9), 6802–6822.

Elling, R. P., Stein, S., Stein, C. A., & Keller, G. R. (2020). Tectonic implications of the gravity signatures of the Midcontinent Rift and Grenville Front. *Tectonophysics*, *778*, 228369.

Faleide, J. I., Tsikalas, F., Breivik, A. J., Mjelde, R., Ritzmann, O., Engen, O., et al. (2008). Structure and evolution of the continental margin off Norway and the Barents Sea. *Episodes*, *31*(1), 82–91.

Franke, D., Neben, S., Ladage, S., Schreckenberger, B., & Hinz, K. (2007). Margin segmentation and volcano-tectonic architecture along the volcanic margin off Argentina/Uruguay, South Atlantic. *Marine Geology*, *244*(1–4), 46–67.

Frizon de Lamotte, D., Fourdan, B., Leleu, S., Leparmentier, F., & de Clarens, P. (2015). Style of rifting and the stages of Pangea breakup. *Tectonics*, *34*(5), 1009–1029.

Gac, S., & Geoffroy, L. (2009). 3D Thermo-mechanical modelling of a stretched continental lithosphere containing localized low-viscosity anomalies (the soft-point theory of plate break-up). *Tectonophysics*, *468*(1–4), 158–168.

Gallahue, M. M., Stein, S., Stein, C. A., Jurdy, D., Barklage, M., & Rooney, T. O. (2020). A compilation of igneous rock volumes at volcanic passive continental margins from interpreted seismic profiles. *Marine and Petroleum Geology*, *122*(August), 104635. https://doi.org/10.1016/j.marpetgeo.2020.104635

Geoffroy, L., Callot, J., Scaillet, S., Skuce, A., Gélard, J. P., Ravilly, M., et al. (2001). Southeast Baffin volcanic margin and the North American-Greenland plate separation. *Tectonics*, *20*(4), 566–584.

Geoffroy, L., Burov, E. B., & Werner, P. (2015). Volcanic passive margins: another way to break up continents. *Scientific Reports*, *5*(1), 1–12.

Gerya, T V. (2013). Initiation of transform faults at rifted continental margins: 3D petrological-thermomechanical modeling and comparison to the Woodlark Basin. *Petrology*, *21*(6), 550–560.

660 Gerya, Taras V. (2013). Three-dimensional thermomechanical modeling of oceanic
661 spreading initiation and evolution. *Physics of the Earth and Planetary Interiors*, *214*,
662 35–52.
663 Greene, J. A., Tominaga, M., Miller, N. C., Hutchinson, D. R., & Karl, M. R. (2017).
664 Refining the Formation and Early Evolution of the Eastern North American Margin:
665 New Insights From Multiscale Magnetic Anomaly Analyses. *Journal of Geophysical*
666 *Research: Solid Earth*. https://doi.org/10.1002/2017JB014308
667 Greene, J. A., Tominaga, M., & Miller, N. C. (2020). Along-Margin Variations in Breakup
668 Volcanism at the Eastern North American Margin. *Journal of Geophysical*
669 *Research: Solid Earth*, e2020JB020040. https://doi.org/10.1029/2020JB020040
670 Hammond, J. O. S., Kendall, J., Stuart, G. W., Keir, D., Ebinger, C., Ayele, A., &
671 Belachew, M. (2011). The nature of the crust beneath the Afar triple junction:
672 Evidence from receiver functions. *Geochemistry, Geophysics, Geosystems*, *12*(12).
673 https://doi.org/10.1029/2011GC003738
674 Hayward, N. J., & Ebinger, C. J. (1996). Variations in the along-axis segmentation of the
675 Afar Rift system. *Tectonics*, *15*(2), 244–257.
676 Holbrook, & Kelemen, P. B. (1993). Large igneous province on the US Atlantic margin
677 and implications for magmatism during continental breakup. *Nature*, *364*(6436),
678 433.
679 Illsley-Kemp, F., Bull, J. M., Keir, D., Gerya, T., Pagli, C., Gernon, T., et al. (2018).
680 Initiation of a proto-transform fault prior to seafloor spreading. *Geochemistry,*
681 *Geophysics, Geosystems*, *19*(12), 4744–4756.
682 https://doi.org/10.1029/2018GC007947
683 Keranen, K., Klemperer, S. L., Gloaguen, R., & Group, E. W. (2004). Three-dimensional
684 seismic imaging of a protoridge axis in the Main Ethiopian rift. *Geology*, *32*(11),
685 949–952.
686 Klingelhoefer, F., Labails, C., Cosquer, E., Rouzo, S., Geli, L., Aslanian, D., et al.
687 (2009). Crustal structure of the SW-Moroccan margin from wide-angle and
688 reflection seismic data (the DAKHLA experiment) Part A: Wide-angle seismic
689 models. *Tectonophysics*, *468*(1–4), 63–82.
690 https://doi.org/10.1016/j.tecto.2008.07.022
691 Klitgord, K. D., & Schouten, H. (1986). Plate kinematics of the central Atlantic. *The*
692 *Western North Atlantic Region*.
693 Koopmann, H., Franke, D., Schreckenberger, B., Schulz, H., Hartwig, A., Stollhofen, H.,
694 & di Primio, R. (2014). Segmentation and volcano-tectonic characteristics along the
695 SW African continental margin, South Atlantic, as derived from multichannel
696 seismic and potential field data. *Marine and Petroleum Geology*, *50*, 22–39.
697 Korenaga, J., Kelemen, P. B., & Holbrook, W. S. (2002). Methods for resolving the
698 origin of large igneous provinces from crustal seismology. *Journal of Geophysical*
699 *Research: Solid Earth*, *107*(B9), ECV-1.
700 LASE Study Group, L. S. (1986). Deep structure of the US East Coast passive margin
701 from large aperture seismic experiments (LASE). *Marine and Petroleum Geology*,
702 *3*(3), 234–242.
703 Luckie, T. W. (2017). Insights on magmatic addition beneath the mid-Atlantic Coastal
704 Plain from crustal seismic refraction data.
705 Lynner, C., Van Avendonk, H. J. A., Bécel, A., Christeson, G. L., Dugan, B., Gaherty, J.

B., et al. (2019). The Eastern North American Margin Community Seismic Experiment: An Amphibious Active-and Passive-Source Dataset. *Seismological Research Letters*.
Marzen, R. E., Shillington, D. J., Lizarralde, D., Knapp, J. H., Heffner, D. M., Davis, J. K., & Harder, S. H. (2020). Limited and localized magmatism in the Central Atlantic Magmatic Province. *Nature Communications*, *11*(1), 1–8. https://doi.org/10.1038/s41467-020-17193-6
Marzoli, A., Callegaro, S., Dal Corso, J., Davies, J. H. F. L., Chiaradia, M., Youbi, N., et al. (2018). The Central Atlantic magmatic province (CAMP): a review. In *The Late Triassic World* (pp. 91–125). Springer. https://doi.org/10.1007/978-3-319-68009-5
Muirhead, J. D., Kattenhorn, S. A., Lee, H., Mana, S., Turrin, B. D., Fischer, T. P., et al. (2016). Evolution of upper crustal faulting assisted by magmatic volatile release during early-stage continental rift development in the East African Rift. *Geosphere*, *12*(6), 1670–1700.
Museur, T., Graindorge, D., Klingelhoefer, F., Roest, W. R., Basile, C., Loncke, L., & Sapin, F. (2021). Deep structure of the Demerara Plateau: From a volcanic margin to a Transform Marginal Plateau. *Tectonophysics*, *803*, 228645.
Reuber, K. R., Pindell, J., & Horn, B. W. (2016). Demerara Rise, offshore Suriname: Magma-rich segment of the Central Atlantic Ocean, and conjugate to the Bahamas hot spot. *Interpretation*, *4*(2), T141–T155.
Scholz, C. A., Shillington, D. J., Wright, L. J. M., Accardo, N., Gaherty, J. B., & Chindandali, P. (2020). Intrarift fault fabric, segmentation, and basin evolution of the Lake Malawi (Nyasa) Rift, East Africa. *Geosphere*, *16*(5), 1293–1311.
Schouten, H., Klitgord, K. D., & Whitehead, J. A. (1985). Segmentation of mid-ocean ridges. *Nature*, *317*(6034), 225–229.
Shillington, D., Bécel, A., Hornbach, M., Lizarralde, D., Magnani, M. B., Van Avendonk, H., et al. (2014). Processed multichannel seismic data off North Carolina and Virginia, acquired during R/V Marcus G. Langseth expedition MGL1408 (2014) as part of the Eastern North America Community Seismic Experiment (ENAM). Interdisciplinary Earth Data Alliance (IEDA), doi.
Shuck, B., Van Avendonk, H. J. A., & Bécel, A. (2019). The role of mantle melts in the transition from rifting to seafloor spreading offshore eastern North America. *Earth and Planetary Science Letters*, *525*, 115756.
Taylor, B., Goodliffe, A., Martinez, F., & Hey, R. (1995). Continental rifting and initial sea-floor spreading in the Woodlark Basin. *Nature*, *374*(6522), 534–537.
Taylor, B., Goodliffe, A., & Martinez, F. (2009). Initiation of transform faults at rifted continental margins. *Comptes Rendus Geoscience*, *341*(5), 428–438.
Thomas, W. A. (2006). Tectonic inheritance at a continental margin. *GSA Today*, *16*(2), 4–11.
Thybo, H, & Nielsen, C. A. (2009). Magma-compensated crustal thinning in continental rift zones. *Nature*, *457*(7231), 873–876.
Thybo, Hans, & Artemieva, I. M. (2013). Moho and magmatic underplating in continental lithosphere. *Tectonophysics*, *609*, 605–619.
Tréhu, A. M., Ballard, A., Dorman, L. M., Gettrust, J. F., Klitgord, K. D., & Schreiner, A. (1989). Structure of the lower crust beneath the Carolina Trough, US Atlantic continental margin. *Journal of Geophysical Research: Solid Earth*, *94*(B8), 10585–

10600.
Van Avendonk, H., Shillington, D. J., Holbrook, W. S., & Hornbach, M. J. (2004). Inferring crustal structure in the Aleutian island arc from a sparse wide-angle seismic data set. *Geochemistry, Geophysics, Geosystems*, *5*(8).
Van Avendonk, H., (2015). Ocean bottom seismometer data, updated with relocated instrument coordinates, off North Carolina and Virginia, acquired during R/V Endeavor expedition EN546 (2014) as part of the Eastern North America Community Seismic Experiment (ENAM). IEDA. doi:10.1594/IEDA/500017
White, R. S., Smith, L. K., Roberts, A. W., Christie, P. A. F., & Kusznir, N. J. (2008). Lower-crustal intrusion on the North Atlantic continental margin. *Nature*, *452*(7186), 460–464.
Wyer, P., & Watts, A. B. (2006). Gravity anomalies and segmentation at the East Coast, USA continental margin. *Geophysical Journal International*, *166*(3), 1015–1038.